Efficient numerical procedure for the determination of the wave function-independent terms in longitudinal optical phonon scattering rates formulated in the Fourier domain

X. Lü[1] · **L. Schrottke[1]** · **H. T. Grahn[1]**

Abstract A recently developed Fourier-transform-based formulation of the longitudinal optical phonon scattering rates in heterostructures allows us to separate the wave functions from multidimensional integrals, which depend on the intersubband transition energy, the chemical potential, and the electron temperature. Here, we discuss an efficient determination of these integrals and an automatic fitting procedure in order to provide a compact table of pre-calculated integrals. As a result, computation times on a scale of minutes for the scattering rates are achieved for any reasonable set of parameters.

Keywords Longitudinal optical phonon · Scattering rates · Adaptive method · Heterostructures

1 Introduction

The interaction between electrons and phonons plays an important role for the carrier transport and the optical properties in semiconductor heterostructures such as quantum-cascade lasers (QCLs) [1–5]. An efficient determination of the scattering rates is crucial not only for an understanding of the underlying physics, but also for optimizing the design strategy and for improving the device performance

✉ X. Lü
lue@pdi-berlin.de

L. Schrottke
lutz@pdi-berlin.de

H. T. Grahn
htgrahn@pdi-berlin.de

[1] Paul-Drude-Institut für Festkörperelektronik, Leibniz-Institut im Forschungsverbund Berlin e. V., Hausvogteiplatz 5–7, 10117 Berlin, Germany

of QCLs. The complexity of the QCL structures leads to a large computation time for the simulation of the transport and optical properties. In particular, the design of these devices requires a balance between accuracy and computation time. For this balance, a suitable method for the calculation of electron–longitudinal optical (LO) phonon scattering rates is necessary. Recently, a method based on the formulation in the Fourier domain has been shown to facilitate the efficient simulation of the properties of heterostructures [6–8] by decreasing the computation time by one order of magnitude compared to a similar model formulated in real space. For example, a computation time of about one minute has been achieved for complete gain maps with 100 values for the applied field strength using empirical scattering rates based on an approximation which substitutes the dipole matrix element for the form factor [7,8]. Although this model is applicable to various THz QCL structures as shown in Ref. [9], it fails in some cases, e.g., when transitions between states of similar parity become important. Therefore, realistic electron–LO phonon scattering rates have to be used. In the Fourier domain, the expressions for the total intersubband rates [8], i.e., the rates averaged over the intrasubband distributions, can be separated into (the Fourier components of) the wave functions and rather complex integrals. In this paper, we present an efficient numerical method to *automatically* create tables of pre-calculated values for these integrals.

2 Determination of the longitudinal optical phonon scattering rates

The electron–LO phonon scattering rate for the transition from subband n to subband j in the Fourier domain is given by

$$T_{jn} = \frac{e^2 E_{\mathrm{LO}}}{4\pi\hbar}\left(\frac{1}{\epsilon_\infty} - \frac{1}{\epsilon_s}\right)$$
$$\times \sum_{a,mlm'l'} \lambda_m^{ja*}\lambda_l^{na}\lambda_{m'}^{ja}\lambda_{l'}^{na*}F_I, \tag{1}$$

where e denotes the electron charge, E_{LO} the LO phonon energy, $\hbar$ Planck's constant, $\epsilon_{\infty(s)}$ the high-frequency (static) dielectric constant, λ_m^{ja} the Fourier components of the wave functions, $a = 1$ or 2 the band indices for a two-band pseudo $\mathbf{k}\cdot\mathbf{p}$ model, and m, l, m', l' the indices of the Fourier components [8]. F_I is a function of the transition energy $E_{nj} = E_n - E_j$, where E_n and E_j refer to the energy of the n-th and j-th states, respectively. Furthermore, it depends on the chemical potential μ_n (μ_j), the electron temperature T_n (T_j), and the energy uncertainty $\widetilde{E}$ [10]. The form of F_I is rather intricate as shown by Eqs. (15)–(17) in Ref. [8]. However, it can be reduced to two three-dimensional integrals F_{II}^ν ($\nu = 0, 1$) as discussed in Ref. [8] with the energy variables normalized by $\widetilde{E}$, e.g., $\bar{E}_q = E_q/\widetilde{E}$

$$F_{II}^\nu = \int_0^{\bar{E}_q^{\max}} \int_0^{\bar{E}_{n0}^{\max}} \int_0^{2\pi} G^\nu \, d\phi_n \, d\bar{E}_{n0} \, d\bar{E}_q, \tag{2}$$

containing the integrand

$$G^\nu = \frac{1}{\ln\left(1 + e^{\bar{\mu}_n/\bar{E}_{T_n}}\right)} \frac{1}{\bar{\Delta}_{lm} + \bar{E}_q}\left(\frac{1 - e^{-\sqrt{\bar{E}_q}\sqrt{\bar{L}}}}{\sqrt{\bar{E}_q}\sqrt{\bar{L}}}\right)^\nu$$
$$\times f_n(1 - f_j)e^{-2\left(\bar{E}_{ab}^{em}\pm\sqrt{\bar{E}_{n0}}\sqrt{\bar{E}_q}\cos(\phi_n) - \frac{1}{2}\bar{E}_q\right)^2}, \tag{3}$$
$$f_n = \frac{1}{1 + e^{(\bar{E}_{n0} - \bar{\mu}_n)/\bar{E}_{T_n}}}, \tag{4}$$

with k_B denoting Boltzmann's constant, $\bar{E}_{n0}$ the normalized kinetic energy, f_n and f_j the Fermi–Dirac distribution for energies $\bar{E}_{n0}$ and $\bar{E}_{j0}^{-/+}$, m^* the electron effective mass, L_z the size of the simulation cell, $\bar{E}_{T_n} = k_B T_n/\widetilde{E}$, $\bar{E}_q = (\hbar q_\parallel)^2/(2m^*\widetilde{E})$, $\bar{E}_{ab}^{em} = (\bar{E}_{nj} \mp \bar{E}_{\mathrm{LO}})/2$, $\bar{E}_{j0}^{-/+} = \bar{E}_{n0} + \bar{E}_q \mp \sqrt{\bar{E}_{n0}}\sqrt{\bar{E}_q}\cos(\phi_n)$, $\bar{\Delta}_{lm} = 4\pi^2(l - m)^2/\bar{L}$, $\bar{L} = 2m^*\widetilde{E}L_z^2/\hbar^2$, $q_\parallel$ the in-plane component of the phonon wave vector, and ϕ_n the angle between the in-plane electron and the phonon momentum. The negative and positive signs in the definitions of $\bar{E}_{ab}^{em}$ and $\bar{E}_{j0}^{-/+}$ correspond to phonon emission (em) and phonon absorption (ab), respectively. For practical reasons, we include a factor $1/\ln\left(1 + e^{\bar{\mu}_n/\bar{E}_{T_n}}\right)$ in the integral F_{II}^ν as given by Eq. (20) in Ref. [8]. In order to obtain the scattering rates, we need to determine the integral F_{II}^ν.

The determination of F_{II}^ν is rather challenging since the exponential function leads to sharply spiked integrands. This type of integral requires a large calculation time in order to

achieve an acceptable accuracy. Since F_{II}^ν is not suitable for a fast calculation during any self-consistent computation, it is useful to automatically generate tables containing the values of F_{II}^ν for the parameter set $(\mathcal{P}) = (\bar{E}_{ab}^{em}, \bar{\mu}_n, \bar{\mu}_j, T_n, T_j, \bar{L})$ in advance to be employed in the self-consistent procedure. We found that a fitting function F_{II}^ν can be used to decompose the scattering rates in parts [8], which allows for a reduced computation time. By setting $y = \ln(\bar{\Delta}_{lm})$, the rational function F_{app}^ν as defined by

$$F_{app}^\nu = \frac{1}{A_\nu + B_\nu e^{y/2} + C_\nu e^y}, \tag{5}$$

can satisfy this requirement [8], i.e.,

$$\sum_{mlm'l'} \lambda_m^{ja*}\lambda_l^{na}\lambda_{m'}^{ja}\lambda_{l'}^{na*}F_I \approx \mathcal{T}_1 + \mathcal{T}_2, \tag{6}$$

with

$$\mathcal{T}_1 \propto \left|\sum_{ml}\lambda_m^{ja*}\lambda_l^{na}F_{app}^1\right|^2,$$
$$\mathcal{T}_2 \propto \sum_{mlm'}\lambda_m^{ja*}\lambda_l^{na}\lambda_{m'}^{ja}\lambda_{l-m+m'}^{na*}F_{app}^0, \tag{7}$$

where A_ν, B_ν, and C_ν are the fitting parameters. The fitting function F_{app}^ν is not only of a rather simple form, but also helpful to reduce the dimension of the parameter space for the table of the pre-calculated values of the integrals and allows for a reduction of the number of summands from N_F^4 [cf. Eq. (6)] to N_F^3 [cf. Eq. (7)] with N_F denoting the number of Fourier components of the wave functions.

3 Numerical integration and fitting procedure

In order to generate the table for various combinations of all the energy-related parameters for F_{II}^ν, an efficient and *automatic* evaluation of F_{II}^ν is crucial. The position and shape of the sharp features of F_{II}^ν depend strongly on the specific parameters. Figure 1 shows exemplarily the integrand G^1 as a function of ϕ_n. For many parameter combinations, in particular for larger values of $\bar{E}_{n0}$, the value of G^1 is close to zero for a wide range of ϕ_n, and we clearly observe two sharp peaks. For the integration of G^ν over a large range, these sharp features require a large number of nodes for a sufficient accuracy of the multidimensional integrals. For GaAs, we use $\bar{E}_q^{\max} = 8 \times 10^5$ and $\bar{E}_{n0}^{\max} = 7k_B T_n/\widetilde{E}$. Here, $\bar{E}_q^{\max}[= (\hbar q^{\max})^2/(2m^*\widetilde{E})]$ is determined by the electron effective mass (m^*) and the phonon wave vector at the Brillouin zone boundary ($q^{\max}$), while $\bar{E}_{n0}^{\max}$ is defined by the value at which the Fermi–Dirac distribution f_n (f_j) is approximately 10^{-3}. Using conventional methods such as
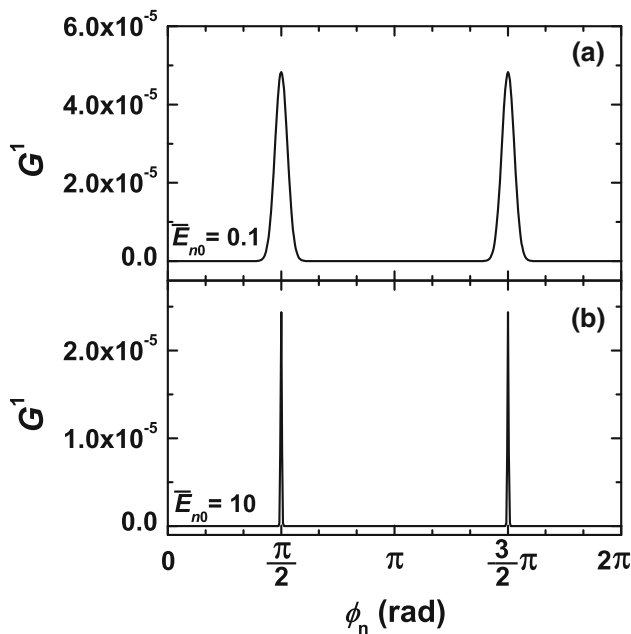
Fig. 1 Integrand G^1 as a function of ϕ_n shown for $\bar{\Delta}_{lm} = 5 \times 10^{-5}$, $\bar{L} = 0.5$, $\bar{\mu}_n = \bar{\mu}_j = 10$, $T_n = T_j = 25$ K, $\bar{E}_{ab}^{em} = 169$, and $\bar{E}_q = 338$ with **a** $\bar{E}_{n0} = 0.1$ and **b** $\bar{E}_{n0} = 10$

Fig. 2 F_{II}^1 as a function of $\ln(\bar{\Delta}_{lm})$ obtained by fitting Eq. (5) without the shift (*dashed line*) and Eq. (8) with the shift (*solid line*) for $\bar{E}_{ab}^{em} = 66$, $\bar{\mu}_n = \bar{\mu}_j = 10$, $T_n = T_j = 50$ K, and $\bar{L} = 0.5$

Simpson's rule may result in unacceptably long computation times. For the integrand with sharp features and the large integration range, an adaptive algorithm is preferred. However, directly applying a Gauss–Kronrod 15-point method to n_d-dimensional integrals requires 15^{n_d} evaluations of the integrand [11]. For an efficient integration method, we apply the algorithm introduced by Berntsen *et al.* [12], which combines product methods with globally adaptive subdivision schemes. By applying this method to s-dimensional integrals, $2^{n_d} + 4n_d(n_d - 1)(n_d - 2)/3 + 6n_d^2 + 2n_d + 1$ (77 for $n_d = 3$) evaluations of the integrand are required, which is much less than the number for the Gauss–Kronrod 15-point method (3,375 for $n_d = 3$). It is one of the few viable approaches to obtain a high precision (relative accuracy much better than 10^{-3}) for an integral dimension $n_d \leq 10$ [13]. Here, we use the Fortran code DCUHRE [14], which is also suitable for parallel computing. Due to a large range of the parameter space ($\mathcal{P}$), a general Fortran code for an automatic determination of the integrals for all the possible parameter combinations is necessary. We use the calculated integrals as the input for a fitting procedure, which generates the table of the energy-related terms A_ν, B_ν, and C_ν.

For the fitting procedure, we apply the Levenberg–Marquardt method according to Ref. [15], which is an efficient method with strong convergence properties. The shape of the fitting function F_{app}^ν is similar to the sigmoidal function $1/(1 + e^{-x})$ or the hyperbolic tangent function $\tanh(x)$. However, the scattering rates T_{jn} cannot be decomposed using $1/(1 + e^{-x})$ or $\tanh(x)$. As discussed
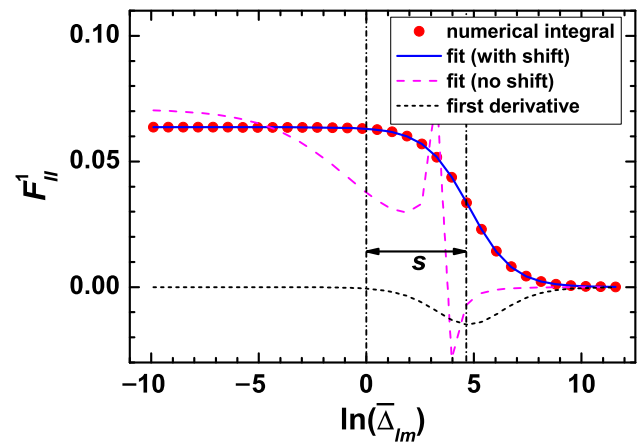
in Sec. 2 [cf. Eqs. (5)–(7)], the use of F_{app}^ν as the fitting function allows us to decompose T_{jn} and to reduce the number of the summands necessary for the determination of T_{jn}. However, using directly the function F_{app}^ν to obtain a good fit would require suitable initial guess values of A_ν, B_ν, and C_ν, which depend strongly on the positions of the inflection points of F_{II}^ν. These guess values change over a very wide range for different parameter sets, which are inconvenient for an automatic fitting of a large number ($>10^6$) of parameter sets. Therefore, we introduce the shift s on y, which is determined by the position of the inflection point of F_{II}^ν (minimum of the first derivative of the numerical integral) so that the inflection points of the functions are shifted close to zero on the abscissa, while the initial guess values can be fixed ($A_\nu = B_\nu = C_\nu$) for all parameter sets. This shift is beneficial for the *automatic* fitting of a large number of integrals with variable parameters. Using the fitting function with the shift

$$F_{app}^{\nu,s} = \frac{1}{A_\nu + B_{\nu,s}e^{(y-s)/2} + C_{\nu,s}e^{y-s}}, \quad (8)$$

we found that the fitting results agree well with the numerical integrals as a function of $\ln(\bar{\Delta}_{lm})$ for all the calculated parameter combinations. Figure 2 shows exemplarily the fit for the parameter set $\bar{E}_{ab}^{em} = 66$, $\bar{\mu}_n = \bar{\mu}_j = 10$, $T_n = T_j = 50$ K, and $\bar{L} = 0.5$. The initial guess values are set to $A_1 = B_1 = C_1 = 1$. For the result using Eq. (5) *without* the shift s, the shape of the fit is very different from the actual result (dashed line in Fig. 2). In contrast, the fit using Eq. (5) *with* the shift s (solid line in Fig. 2) is rather good. Since both, the small values of F_{app}^ν and the high-order Fourier components, i.e., large values of $\bar{\Delta}_{lm}$, contribute very little to the scattering rates, we define a normalized error in order to evaluate the quality of the fit. This normalized error

is the maximum of the absolute error ($|F_{II}^1 - F_{app}^1|$) over the entire range of $\bar{\Delta}_{lm}$ divided by the maximum of the F_{II}^1-$\ln(\bar{\Delta}_{lm})$ curve. For the case shown in Fig. 2, the normalized error is below 0.3%.

To verify the validity of our method, we implemented the fitting procedure and applied it to a large number of parameter combinations. Figure 3 shows the results of the fit using $F_{app}^{1,s}$ for $\bar{\mu}_n = \bar{\mu}_j = -20$ in comparison to the numerical integrals for several parameter combinations of $\bar{E}_{ab}^{em}$, T_n, T_j, and $\bar{L}$. Figure 3a depicts the results for $\bar{E}_{ab}^{em} = 3.87$ and different values of $\bar{L}$, while Fig. 3b shows the results for $\bar{L} = 1$ and different values of $\bar{E}_{ab}^{em}$. In Fig. 3a, b, the electron temperature $T_n = T_j$ is set to 100 K. Due to the similar shape of the curves with variable $\bar{L}$ in Fig. 3a, the value of the shift is fixed ($s = 1.01$). Figure 3c shows the temperature-dependent results for $\bar{E}_{ab}^{em} = 3.87$ and $\bar{L} = 1$. Figure 3d, e show the range of the shift s as a function of $\bar{E}_{ab}^{em}$ and $T = T_n = T_j$. In order to create the table to be used for the determination of the scattering rates for each electron temperature, e.g., $T_n = T_j = 25, 50, 75$, and 100 K, we apply the parameter set: $|\bar{E}_{ab}^{em}| \leq 430$, $-100 \leq \bar{\mu}_n = \bar{\mu}_j \leq 50$, and $0.5 \leq \bar{L} \leq 16,384$. By automatic fitting a large number of curves in the range defined above, we found that the fits agree well with the results of the numerical integration in the range of $-9.9 \leq \ln(\bar{\Delta}_{lm}) \leq 11.5$. For $|\bar{E}_{ab}^{em}| > 2$, the normalized error is below 2.3% for all parameter sets and decreases with the increasing value of $|\bar{E}_{ab}^{em}|$. However, when the energy is close to the phonon resonance ($|\bar{E}_{ab}^{em}| < 2$), the normalized error increases. Since in this case $F_{app}^1 < F_{II}^1$, which coincides with a necessary reduction of the scattering rates as discussed in Ref. [8], the increase of the normalized error has a negligible effect on the final result. In the end, we obtain the table including all the information for a fast evaluation of F_{II}^ν using a linear interpolation for the actual parameters if these lie between the data points of the table.

4 Discussion and resulting procedure

The energy-related terms F_{II}^ν are directly obtained from the table through Eq. (5), which is independent of the self-consistent procedure, so that the total simulation time is only increased by a factor of about 6 compared to the empirical model in the Fourier domain and is still twice as fast as the merely empirical model in real space [7,8]. Finally, we discuss the parameter space in detail. Since we mainly focus on the design of GaAs/Al$_x$Ga$_{1-x}$As THz QCLs, all the parameters are related to Al$_x$Ga$_{1-x}$As. For the effective electron mass, we use $m^*/m_0 = 0.067 + 0.083x$, where m_0 denotes the free electron mass. The conduction band offset of GaAs/Al$_x$Ga$_{1-x}$As can be obtained by assuming a 65:35 ratio between the conduction and valence band offsets [16]
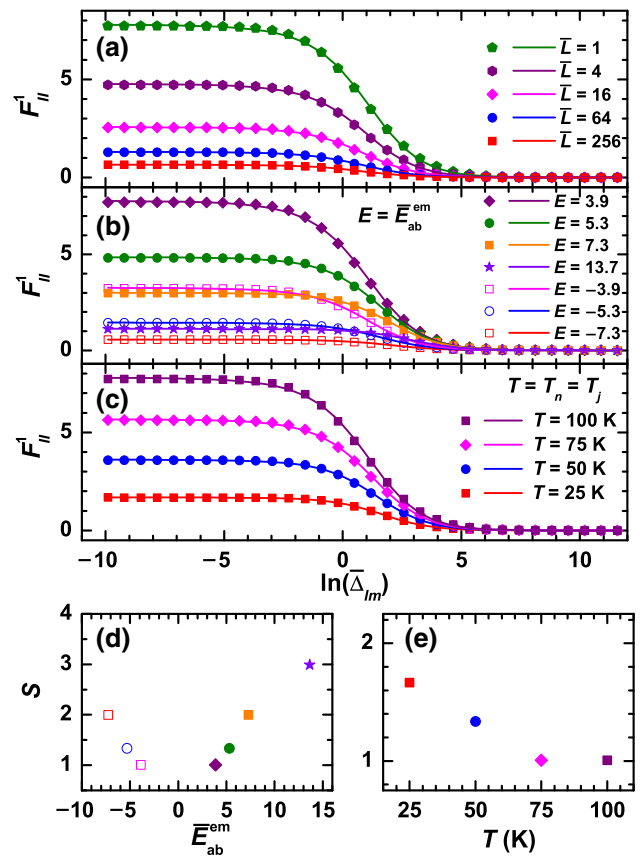

Fig. 3 F_{II}^1 as a function of $\ln(\bar{\Delta}_{lm})$ for **a** $\bar{E}_{ab}^{em} = 3.87$ and $T_n = T_j = 100$ K with variable $\bar{L}$, **b** $\bar{L} = 1$ and $T_n = T_j = 100$ K with variable $\bar{E}_{ab}^{em}$, and **c** $\bar{E}_{ab}^{em} = 3.87$ and $\bar{L} = 1$ with variable T_n and T_j obtained by numerical integration (*dots*) and fits (*solid lines*). The shift s as a function of **d** $\bar{E}_{ab}^{em}$ and **e** $T = T_n = T_j$. The other parameter is $\bar{\mu}_n = \bar{\mu}_j = -20$

$$V_{CB} = (1.109x - 0.934x^2 + 0.851x^3) \text{ eV}. \qquad (9)$$

For $x = 0.25$, the offset is equal to 0.232 eV, while for $x = 1$, the offset is 1.026 eV. As discussed in Ref. [17], the height of the injection barriers in GaAs/AlAs THz QCLs is expected to be less than 80% of the maximum value due to interface grading [7]. Therefore, we may apply $0.8V_{CB}^{max}$ as the maximum of E_{nj}, and the corresponding maximum value for $E_{ab}^{em}[= (E_{nj} \mp E_{LO})/2]$ is about 0.43 eV, which is much larger than the energy of the LO phonon in GaAs (36 meV or 8.8 THz). The chemical potential is [3]

$$\mu_n = k_B T_n \ln\left[\exp\left(\frac{\pi \hbar^2 n^{2D} \rho_{nn}}{m^* k_B T_n} \right) - 1 \right], \qquad (10)$$

where n^{2D} denotes the sheet carrier density and ρ_{nn} the occupation number of the n-th subband. Table 1 gives the calculated chemical potential for different sheet carrier densities and electron temperatures. Here $\rho_{nn}n^{2D} = 1 \times 10^{11}$ and 1×10^{12} cm^{-2} cover the typical range of values for GaAs/Al$_x$Ga$_{1-x}$As THz QCLs. The maximum

Table 1 Chemical potential μ_n and maximum of the kinetic energy $E_{n0}^{\max}$ for different values of n^{2D} and T_n

$\rho_{nn} n^{2D}$ (cm^{-2})	T_n (K)	μ_n (meV)	$E_{n0}^{\max}$ (meV)
1×10^{11}	10	3.6	9.5
	50	1.1	30.8
	100	-5.7	53.8
	300	-49.4	129.2
	400	-76.3	161.7
1×10^{12}	10	35.7	41.7
	50	35.7	65.5
	100	35.6	95.1
	300	28.2	206.8
	400	20.6	258.7

kinetic energy $E_{n0}^{\max}$ is defined by the value for which the Fermi–Dirac distribution is about 10^{-3}. We consider -100 meV $\leq \mu_n \leq 50$ meV and 10 K $\leq T_n \leq 400$ K. For $\bar{L}$ [$= \tilde{E} L_z^2 / (570$ meV nm$^2)$], we assume $L_z < 960$ nm and $1 \leq \tilde{E} \leq 10$ meV so that we obtain a range for $\bar{L}$ of $0.5 \leq \bar{L} < 17,000$.

Within this range for the parameter set $(\mathcal{P}) = (\bar{E}_{ab}^{em}, \bar{\mu}_n, \bar{\mu}_j, T_n, T_j, \bar{L})$, a number $N_\mathcal{P}$ for $\bar{E}_{ab}^{em}, \bar{\mu}_n, \bar{\mu}_j, T_n, T_j$, and $\bar{L}$ is selected to guarantee a limited storage requirement for the table files. The steps for $\bar{\mu}_n, \bar{\mu}_j, T_n$, and T_j are set on a linear scale, while for $\bar{E}_{ab}^{em}$ and $\bar{L}$ we use a logarithmic scale. As an example, for a fixed electron temperature, $N_{\bar{E}_{ab}^{em}} = 40$ and $N_{\bar{\mu}_n} = N_{\bar{\mu}_j} = N_{\bar{L}} = 16$, the generated table file contains 163,840 triples of A_ν, B_ν ($= B_{\nu,s} e^{-s/2}$), and C_ν ($= C_{\nu,s} e^{-s}$) with a size of 8.5 MB, which can be quickly loaded by the main program for the calculation of the scattering rates. When performing the interpolation, these values for $N_\mathcal{P}$ allow for an error which is of the same order of magnitude as the maximum normalized error due to the fitting procedure.

The determination of the scattering rates is separated into two parts. Before any self-consistent calculation, the table of the values for A_ν, B_ν, and C_ν is created once for all future simulations. First, we calculate the numerical integrals as functions of $\bar{\Delta}_{lm}$ for all the parameter combinations using the adaptive algorithm. Second, we fit the pre-calculated curves automatically using the Levenberg–Marquardt method. Third, we obtain the tables for A_ν, B_ν, and C_ν for different electron temperatures. For the self-consistent procedure, we assume the same electron temperatures in all subbands and combine LO phonon scattering rates [Eq. (1)] with our self-consistent Fourier domain model as described in Ref. [7]. For parameter sets which are not included in the table files, multidimensional interpolation is applied on the calculated A_ν, B_ν, and C_ν in order to obtain the actual value of G^ν. By applying this method, it is pos-

sible to calculate the influence of electron temperatures and carrier densities on the transport and optical properties of complex heterostructures on a time scale of minutes, which is beneficial for the efficient design of THz QCLs [8].

5 Conclusions

We have presented an efficient method to determine the wave function-independent component for the longitudinal optical phonon scattering rates formulated in the Fourier domain using a numerical determination of the multidimensional integrals and an automatic fit to these pre-calculated integrals. This method allows us to fully decompose the energy-dependent component from the self-consistent procedure in order to achieve computation times for entire gain maps and current density-applied field strength curves on a time scale of a few minutes using standard work stations. It is a powerful tool for a realistic simulation of the properties and the design of complex heterostructures such as QCLs with short computation times.

References

1. Faist, J., Capasso, F., Sivco, D.L., Sirtori, C., Hutchinson, A.L., Cho, A.Y.: Quantum cascade laser. Science **264**, 553–556 (1994). doi:10.1126/science.264.5158.553
2. Köhler, R., Tredicucci, A., Beltram, F., Beere, H.E., Linfield, E.H., Davies, A.G., Ritchie, D.A., Iotti, R.C., Rossi, F.: Terahertz semiconductor-heterostructure laser. Nature **417**, 156–159 (2002). doi:10.1038/417156a
3. Harrison, P.: Quantum Wells, Wires and Dots: Theoretical and Computational Physics of Semiconductor Nanostructures. Wiley, Chichester (2005)
4. Williams, B.S.: Terahertz quantum-cascade lasers. Nat. Photon. **1**, 517–525 (2007). doi:10.1038/nphoton.2007.166
5. Jirauschek, C., Kubis, T.: Modeling techniques for quantum cascade lasers. Appl. Phys. Rev. **1**, 011307 (2014). doi:10.1063/1.4863665
6. Lü, X., Schrottke, L., Luna, E., Grahn, H.T.: Efficient simulation of the impact of interface grading on the transport and optical properties of semiconductor heterostructures. Appl. Phys. Lett. **104**, 232106 (2014). doi:10.1063/1.4882653
7. Schrottke, L., Lü, X., Grahn, H.T.: Fourier transform-based scattering-rate method for self-consistent simulations of carrier transport in semiconductor heterostructures. J. Appl. Phys. **117**, 154309 (2015). doi:10.1063/1.4918671
8. Lü, X., Schrottke, L., Grahn, H.T.: Fourier-transform-based model for carrier transport in semiconductor heterostructures: Longitudinal optical phonon scattering. J. Appl. Phys. **119**, 214302 (2016). doi:10.1063/1.4952741
9. Schrottke, L., Giehler, M., Wienold, M., Hey, R., Grahn, H.T.: Compact model for the efficient simulation of the optical gain and transport properties in THz quantum-cascade lasers. Semi-

cond. Sci. Technol. **25**, 045025 (2010). doi:10.1088/0268-1242/25/4/045025

10. Taj, D., Iotti, R.C., Rossi, F.: Microscopic modeling of energy relaxation and decoherence in quantum optoelectronic devices at the nanoscale. Eur. Phys. J. B **72**, 305–322 (2009). doi:10.1140/epjb/e2009-00363-4

11. Arumugam, K., Godunov, A., Ranjan, D., Terzić, B., Zubair, M.: A memory efficient algorithm for adaptive multidimensional integration with multiple GPUs. In: 20th Annual International Conference on High Performance Computing, pp. 169–175 (2013). doi:10.1109/HiPC.2013.6799120

12. Berntsen, J., Espelid, T.O., Genz, A.: An adaptive algorithm for the approximate calculation of multiple integrals. ACM Trans. Math. Software **17**, 437–451 (1991). doi:10.1145/210232.210233

13. Hahn, T.: Cuba-a library for multidimensional numerical integration. Comput. Phys. Commun. **168**, 78–95 (2005). doi:10.1016/j.cpc.2005.01.010

14. Berntsen, J., Espelid, T.O., Genz, A.: Algorithm 698: Dcuhre: an adaptive multidimensional integration routine for a vector of integrals. ACM Trans. Math. Software **17**, 452–456 (1991). doi:10.1145/210232.210234

15. Press, W.H., Teukolsky, S.A., Vetterling, W.T., Flannery, B.P.: Numerical Recipes in Fortran 90: The art of Parallel Scientific Computing. Press Syndicate of the University of Cambridge, Cambridge (2002)

16. Vurgaftman, I., Meyer, J.R., Ram-Mohan, L.R.: Band parameters for iiiv compound semiconductors and their alloys. J. Appl. Phys. **89**, 5815–5875 (2001). doi:10.1063/1.1368156

17. Schrottke, L., Lü, X., Rozas, G., Biermann, K., Grahn, H.T.: Terahertz GaAs/AlAs quantum-cascade lasers. Appl. Phys. Lett. **108**, 102102 (2016). doi:10.1063/1.4943657